J Mater Sci (2011) 46:7620–7625
DOI 10.1007/s10853-011-5739-6

Splitting and broadening of the emission bands of Y_2O_3:Eu^{3+},Nd^{3+} and its dependence on Nd^{3+} concentration and annealing temperature

Wangdong Liu · Hanchao Wang · Shiping Zhan · Wenbin Li

Received: 22 May 2011 / Accepted: 21 June 2011 / Published online: 29 June 2011

Abstract Although Eu^{3+} ion-doped Y_2O_3 has been extensively used as red phosphors, their color rendering needs to be improved for high-quality illumination and displaying. Here, we show that the emission spectra of Y_2O_3:Eu^{3+} red phosphors can be broadened by the doping of Nd^{3+} ion so that the color rendering capability of Y_2O_3:Eu^{3+} was remarkably enhanced. Y_2O_3:Eu^{3+} and Y_2O_3:Eu^{3+},Nd^{3+} colloidal spheres were synthesized by wet chemical procedure and high-temperature treatment. The fluorescence measurement under the 254 and 380 nm ultraviolet excitation indicates that the 612 nm red emission peak of Eu^{3+} can be splitted into two ones by the doping of Nd^{3+} ion, of which the full width at half maximum (FWHM) is broadened from 4.2 nm to 9.6 nm. By varying the concentration of Nd^{3+} ion, it was determined that the optimal doping concentration of Nd^{3+} ion is of 3 mol% for realizing the strongest emission intensity. The further increase of Nd^{3+} ion exceeding 3 mol% would lead to a concentration quenching phenomenon. The analysis based on XRD spectra and the simplified energy diagram suggested that the doped Nd^{3+} ion not only monitored the growth dynamics, but also took an efficient energy transfer and a cross relaxation process to generate intense emission from Eu^{3+} ion in both of C_2 and S_6 sites, instead of preferable one type of Eu^{3+} site (C_2 or S_6) in the Nd^{3+} undoped sample.

W. Liu (✉) · S. Zhan · W. Li
School of Physics, Hunan University of Science and Technology, Xiangtan 411201, China
e-mail: liuwangdong@hnust.edu.cn

H. Wang
Institute of Modern Physics, Xiangtan University, Xiangtan 411105, China

Introduction

Lanthanide Eu^{3+} ion has been extensively used as emitter and doped into various host materials to generate red light ($\sim$611 nm) by the 4fn electric dipolar transition of $^5D_0$–$^7F_2$. Among these Eu^{3+} ion activated red light materials, Y_2O_3:Eu^{3+} is one of the most important, since the host material Y_2O_3 has high thermal stability, low phonon energy and luminescence quenching rate, and similar physical and chemical properties to the doped Eu^{3+} ions [1–5]. Therefore, Y_2O_3:Eu^{3+} has been widely synthesized and applied as red phosphors in the fields of fluorescent lighting, cathode ray tube, field emission display (FED), and plasma display panels (PDP) [1–8].

Although phosphors-based lighting and displaying devices have been widely applied in our daily life, the luminescence spectra of most of these devices just covered a portion of the overall visible light, which is some different from the sunshine that covers the whole visible light range (380–780 nm). Therefore, these artificial lighting sources have worse color recover capability for indoor lighting or displaying [9]. Enlarging the luminescence spectra range of phosphors covered in visible light (close to sunshine) is considered to be an ultimate aim for the application of illumination. In ever synthesized cubic Y_2O_3:Eu^{3+}, just a sharp emission band centered at 611 nm from the electric dipolar transition of $^5D_0$–$^7F_2$ was generated with the full width at half maximum (FWHM) of $\sim$7 nm. Although, the FWHM of $^5D_0$–$^7F_2$ of Eu^{3+} transition in monoclinic Y_2O_3 phase is much broader than that in cubic Y_2O_3 phase [10]. Unfortunately, the monoclinic Y_2O_3 phase has worse stability than cubic one, and its produce needs generally specific synthesis conditions, for instance, high pressure and special apparatus [10]. Therefore, it will be valuable to develop a novel method for

realizing the broad-band red light emission of Eu^{3+} in the stable Y_2O_3 cubic phase. In this study, we show that the red emission band of Y_2O_3:Eu^{3+} under UV excitation can be efficiently broadened by doping Nd^{3+} ion. Meanwhile, the obvious splitting of the emission bands of Eu^{3+} ion has also been observed by doping Nd^{3+} ion. The analysis based on the microstructure detection, fluorescent spectra and simplified energy level diagram indicates that the energy transfer between Eu^{3+}/Nd^{3+} pairs and the variation of crystal field environment of Eu^{3+} induced by doping Nd^{3+} ion responded for the splitting and broadening of the emission bands of Eu^{3+} ions in cubic phase Y_2O_3.

Experimental

Samples with the composition of Table 1 were synthesized as follows: rare earth (RE) oxides Y_2O_3, Eu_2O_3, and Nd_2O_3 were dissolved with HNO_3 to produce RE nitrate. The $RE(NO_3)_3$ were re-dispersed in distilled water and stirred for 30 min at room temperature. Subsequently, the $RE(NO_3)_3$ aqueous solution was heated to 60 °C with continuous stirring, and the urea was added. Then, the mixed solution was stirred for 3 h at temperature of 65 °C. Finally, the prepared solution was transferred into a 50 mL autoclave, sealed, and reacted at the temperature of 110 °C for 24 h. After the reaction finished, the products were collected, washed with distilled water and ethanol, and calcined at the temperature of 750 °C for 2 h. For further analysis, part of the as prepared samples was annealed at the temperature of 1000 °C for 2 h. The sample without the doping of Nd^{3+} was synthesized with the same procedure. Scanning electron microscopy (SEM) images were recorded using a FE-SEM JEOL JSM-6700F microscope. X-ray diffraction (XRD) data were recorded on a D/max-3c X-ray diffractometer system with graphite monochromatized Cu Kα irradiation ($\lambda = 0.15418$ nm). Fluorescence spectra were measured with a Jobin–Yvon U1000 spectrophotometer under the excitation of a 254 or 380 nm UV lamp. Excitation spectra were recorded at room temperature using a Hitachi F-4500 spectrophotometer.

Results and discussion

Yttrium oxide has two types of crystal lattice structures, i.e., Cubic and monoclinic [10]. It is well-known that the cubic phase Y_2O_3 has higher chemical and physical stability than the monoclinic one. Figure 1 shows the XRD spectra of (a) Y_2O_3:Eu^{3+} and (b) Y_2O_3:Eu^{3+},3 mol%Nd^{3+}. It is quite clear that the XRD peaks of both Y_2O_3:Eu^{3+} and Y_2O_3:Eu^{3+},3 mol%Nd^{3+} can be easily assigned to the cubic Y_2O_3 phase (JCPDS card no. 65-3178). It is noted

Table 1 The initial composition with molar ratio, the annealing temperature and time, and the excitation wavelength

Sample	Y^{3+}	Eu^{3+}	Nd^{3+}	Annealing (°C/2 h)	Excitation (nm)
1	97	3	0	750	254
2	97	3	0.5	750	254
3	97	3	1	750	254
4	97	3	2	750	254
5	97	3	3	750; 1000	254; 380
6	97	3	5	750	254
7	97	3	7	750	254

that the peaks of XRD spectra of Y_2O_3:Eu^{3+},3 mol%Nd^{3+} is obviously wider than that of Y_2O_3:Eu^{3+}, which implies the difference of particle size between them. According to the previous reports, it can be inferred that the doping Nd^{3+} ion may play a role of crystallizing agents to monitor the nuclear and growth process. In most cases, homogeneous nucleation of solid phases requires a high activation energy barrier and therefore heteronucleation will favorably occur. The doping of Nd^{3+} ion has just supplied such an energy barrier that would promote energetically the heteronucleation of Y_2O_3. The crystal particle size of Y_2O_3:Eu^{3+} and Y_2O_3:Eu^{3+},3 mol%Nd^{3+} can be estimated by Scherrers equation [11]:

$$D = \frac{0.89\lambda}{2\beta\cos\theta}$$

where D represents the crystallite size, λ is the wavelength of Cu Kα irradiation; and β is the corrected half width of the diffraction peak. The calculated crystal particle sizes are equal to 52 nm for Y_2O_3:Eu^{3+} and 38 nm for Y_2O_3:Eu^{3+},Nd^{3+}, respectively, demonstrating the higher nucleation speed and shorter growth time of Y_2O_3:Eu^{3+},Nd^{3+} crystal particles in comparison to Y_2O_3:Eu^{3+}.

Urea co-precipitation method has been successfully used to produce oxide micro and nano spheres, rods, and sheets with desired size and aspect ratio. Figure 2 shows the SEM image of Y_2O_3:Eu^{3+},Nd^{3+} with spherical morphology. The image with higher magnification in the insert of Fig. 2 presents the rather smooth surface of these particles.

Yttrium oxide has two types of crystal lattice sites, i.e., C_2 and S_6, which show different optical properties due to a fact that they have distinct charge compassation and local environmental symmetries [12]. From ever reported results, it can be concluded that the doped fluorescence emitters, such as rare earth ion Eu^{3+}, in cubic Y_2O_3 not only have different fluorescence intensity, but also different fluorescence spectra shape from each other. Therefore, it is clear that the fluorescence spectra shape of Y_2O_3:Eu^{3+} is remarkably depended on the crystal field environment of Eu^{3+} sites. Up to now, much effort has been taken focusing

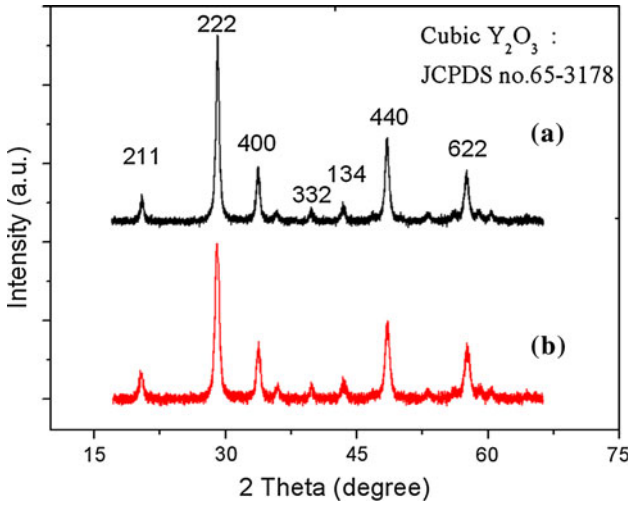

Fig. 1 XRD spectra of **a** Y_2O_3:Eu^{3+} and **b** Y_2O_3:Eu^{3+},3 mol%Nd^{3+}

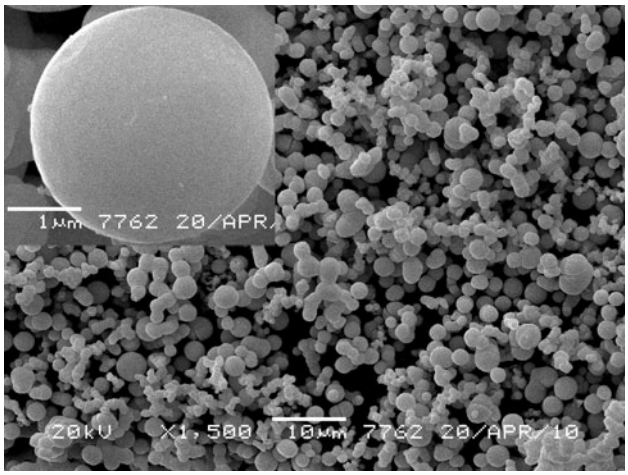

Fig. 2 SEM images of cubic Y_2O_3:Eu^{3+}. The *inset* shows the sphere morphology of a single particle

on the synthesis of rare earth doped Y_2O_3 micro- and nanoparticles with various morphologies, size, and optical properties, for instance, high-temperature solid state reaction, sol–gel techniques, homogeneous precipitation, microemulsion, thermal hydrolysis, combustion synthesis, chemical vapor synthesis, spray pyrolysis, and flame spray pyrolysis [12–18]. For these synthesis methods, it is commonly regarded that the reaction time, temperature, and concentration of raw composition have remarkable influence on the phase structure of the produced Y_2O_3. In this study, it was found that the doping of Nd^{3+} ion into Y_2O_3:Eu^{3+} affects obviously the crystal field environment of Eu^{3+} sites and the distribution probability of Eu^{3+} in C_2 and S_6 sites, and further monitors their fluorescence properties.

Fluorescence spectra of Y_2O_3:Eu^{3+} and Y_2O_3:Eu^{3+}, 3 mol%Nd^{3+} calcined for 750 °C/2 h were measured under the 254 nm UV excitation and shown in Fig. 3a. From the fluorescence spectra of Y_2O_3:Eu^{3+}, it was observed that red emission centered at 612 nm and yellow emission centered at 592 nm dominate the fluorescent spectra, which can be easily assigned to 4f-electronic transitions of Eu^{3+} ions, i.e., $^5D_0$–$^7F_2$ electric dipolar transition and $^5D_0$–$^7F_1$ magnetic dipolar transition, respectively [19–21]. Interestingly, the fluorescent spectra of Y_2O_3:Eu^{3+},3 mol%Nd^{3+} is obviously different from those of Y_2O_3:Eu^{3+}: first, the $^5D_0$–$^7F_2$ emission peak has a red shift of 2 nm; second, a new peak centered at 621 nm arises; lastly, the band width of the red emission was greatly broadened. Based on energy level gap values and reported fluorescence spectra of Nd^{3+} ion, it excludes the

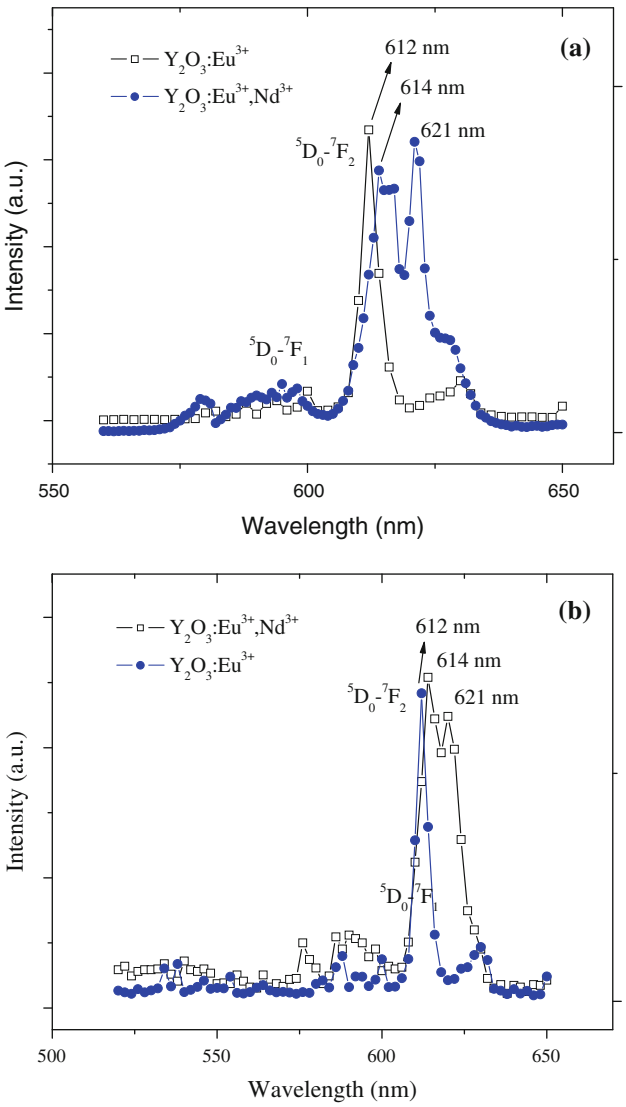

Fig. 3 Fluorescence spectra measured under the 254 nm UV excitation of **a** Y_2O_3:Eu^{3+} and Y_2O_3:Eu^{3+}, 3 mol%Nd^{3+} calcined for 750 °C/2 h. **b** Y_2O_3:Eu^{3+} and Y_2O_3:Eu^{3+}, 3 mol%Nd^{3+} calcined for 750 and 1000 °C/2 h

contribution of Nd^{3+} ion to the 621 nm emission peak. Then, it can only be ascribed to the emission of Eu^{3+} ion. Actually, it can be properly addressed if the influence of Nd^{3+} ion on the crystal field environment of Eu^{3+} sites is taken into accounts. As mentioned above, the emission of Eu^{3+} ion is highly dependent on the local crystal environment of Eu^{3+} sites, for instance, symmetry, and coordination. In most cases, the more the type of site symmetries is, the broader the emission band of the doped emitters is. There exist two types of crystallographic sites in cubic Y_2O_3, S_6, and C_2. Although we did not determine which site symmetry mainly contributing to the 614 nm emission peak, it is undoubted that the emission intensity from C_2 site is much higher or lower than that from S_6 site in Y_2O_3:Eu^{3+}, instead of equally to each other. Differentially, after the doping of Nd^{3+} ion, the distribution of Eu^{3+} ion in C_2 and S_6 sites were accordingly tuned so that the emission intensity from C_2 site is almost equal to that from S_6 site in Y_2O_3:Eu, 3 mol%Nd^{3+}. As a result, it was observed from Fig. 3a that the emission peak of $^5D_0$–$^7F_2$ transition of Eu^{3+} in Y_2O_3:Eu^{3+},3 mol%Nd^{3+} splits into two sub-peaks, of which the width (9.6 nm) is much broader than that (4.2 nm) in Y_2O_3:Eu^{3+}.

In order to investigate the influence of heat treatment on the fluorescence properties, Y_2O_3:Eu^{3+},Nd^{3+} and Y_2O_3:Eu^{3+} were both annealed at temperature 1000 °C for 2 h, of which fluorescence spectra were measured and shown in Fig. 3b. In comparison to the fluorescence spectra in Fig. 3a, the 621 nm splitting peak of Y_2O_3:Eu^{3+}, 3 mol%Nd^{3+} was slightly lowered relatively to the 614 nm one. It should be noted that the crystallinity of Y_2O_3:Eu^{3+},3 mol%Nd^{3+} was improved by the heat treatment, which would lower the influence of Nd^{3+} ion on the crystal field of Eu^{3+} sites. Then, it is not difficult to inferred that the remarkable fluorescent spectra variation of Y_2O_3:Eu^{3+},Nd^{3+} is induced by the lowered influence of Nd^{3+} ion on the crystal field of Eu^{3+} sites.

The above crystal structure analysis based on XRD spectra has demonstrated that the doping of Nd^{3+} monitors the nucleation and growth process to affect the crystal structure of the produced samples. Whether this influence is linearly dependent on the Nd^{3+} content? Figure 4 shows that the fluorescent intensity aspect ratio (FIAR) of 621–614 nm Gaussi component increases firstly with increasing Nd^{3+} content, but, decreases as the concentration of Nd^{3+} ions exceeding 3 mol%. For this case, it can be suggested that Nd^{3+} ion plays a role of nucleating agent for the nucleation of Y_2O_3 nanocrystals and subsequently controlling the growth of nucleus to produce favorably the

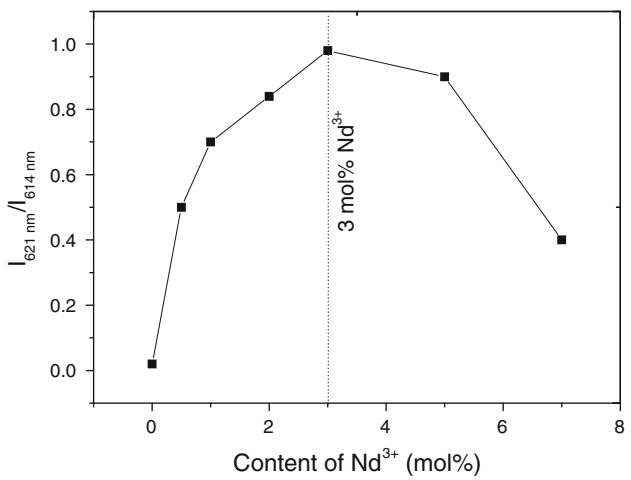

Fig. 4 FIAR of 621–614 nm Gaussi components varying with increasing Nd^{3+} content

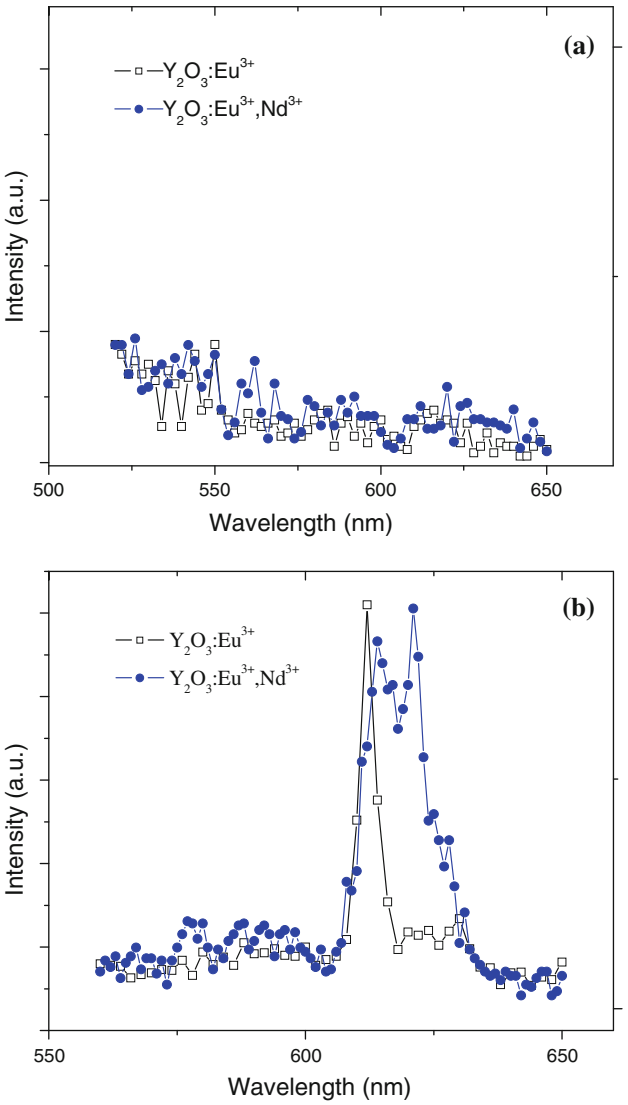

Fig. 5 Fluorescence spectra measured under the 380 nm UV excitation of **a** Y_2O_3:Eu^{3+} and Y_2O_3:Eu^{3+}, 3 mol%Nd^{3+} calcined for 750 °C/2 h. **b** Y_2O_3:Eu^{3+} and Y_2O_3:Eu^{3+}, 3 mol%Nd^{3+} calcined for 750 and 1000 °C/2 h

equal distribution of Eu^{3+} ion in C_2 and S_6 sites in the Y_2O_3 crystal lattices. However, Nd^{3+} ion might prevent the growth of nucleus and destroy this equilibrium distribution as its concentration is higher than a threshold (~3 mol% for the case of this study). Consequently, the FIAR of 621–614 nm Gaussi component decreases with further increasing Nd^{3+} content higher than 3 mol%.

For revealing further the fluorescence properties, Y_2O_3:Eu^{3+} and Y_2O_3:Eu^{3+},Nd^{3+} were excited with longer wavelength UV light (380 nm) and shown in Fig. 5. Interestingly, no emission peak was obviously observed for as prepared Y_2O_3:Eu^{3+} and Y_2O_3:Eu^{3+},3 mol%Nd^{3+} (Fig. 5a), implying their inefficient excitation properties by this long-wavelength UV light. Differentially, the similar fluorescence spectra with those under 254 nm excitation were observed for the annealed Y_2O_3:Eu^{3+} and Y_2O_3:Eu^{3+},3 mol%Nd^{3+} (Fig. 5b), which could be ascribed to better crystallinity of the annealed samples resulting in more efficient photoluminescence.

Based on the simplified energy level diagram of Eu^{3+} and Nd^{3+} in Fig. 6, the influence of Nd^{3+} ion on the excitation and emission process of Eu^{3+} can be properly suggested as follows: as previously described [22], the UV excitation photons were firstly absorbed by the Eu^{3+}–O^{2-} charge transfer (CT) bands, and then relaxed and transferred the energy to the neighbor Eu^{3+} ions for the transition of ground state to higher excited one of Eu^{3+} ion [22]. Generally, only part of the electrons depopulates the ground state to emit light, while the other part takes a multi-phonon relaxation process. For the case of this study, it is suggested that the doping of Nd^{3+} ion has resulted in a cross relaxation of $^5D_0 + {}^4I_{15/2} \rightarrow {}^7F_1 + {}^2D_{3/2}$ for temporary energy reserving so that the efficient emitting

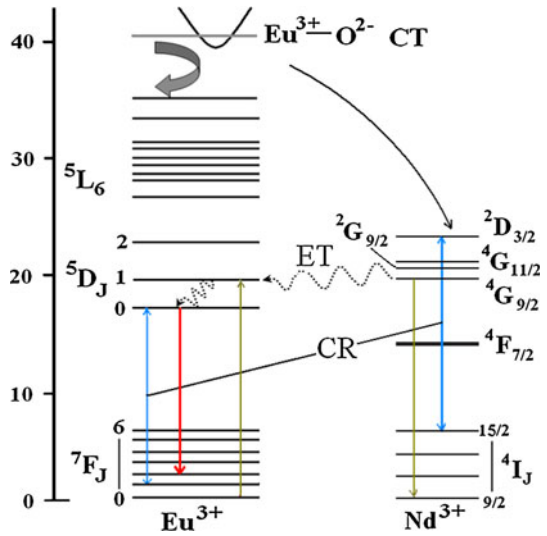

Fig. 6 Simplified energy level diagram of Eu^{3+} and Nd^{3+} and possible excitation and emission mechanisms

electrons of $^5D_0$ level was relatively improved. Moreover, the Nd^{3+} ion may absorb the energy from the Eu^{3+}–O^{2-} CT bands to undergo an efficient energy transfer (ET) process of $^4G_{9/2} + {}^7F_0 \rightarrow {}^4I_{9/2} + {}^5D_1$ to supply the $^5D_1$ energy level of Eu^{3+} ions. As a result, the efficiency from $^5D_0 \rightarrow {}^7F_2$ transition was remarkably enhanced which resulted in strong emission in both of site C_2 and S_6.

Conclusion

In conclusion, Y_2O_3 Y_2O_3:Eu^{3+} and Y_2O_3:Eu^{3+},Nd^{3+} colloidal spheres were successfully produced by combining the wet chemical procedure and high temperature treatment. XRD spectra analysis indicates that the doping of Nd^{3+} ion monitors the growth dynamics of cubic Y_2O_3 phase so that the size of the Eu^{3+} and Nd^{3+}-doped Y_2O_3 crystal particles is smaller than that of only Eu^{3+} doped one. The fluorescence spectra were measured under the 254 and 380 nm ultraviolet excitation that the 612 nm red emission peak of Eu^{3+} was splitted into two ones after the doping of Nd^{3+} ion, of which FWHM is broadened from 4.2 to 9.6 nm. By varying the concentration of Nd^{3+} ion, it was determined that the optimal doping concentration of Nd^{3+} ion is of 3 mol% for realizing the strongest emission intensity. As the content of Nd^{3+} ion exceeding 3 mol%, the concentration quenching phenomenon will occur to eliminate the emission from Eu^{3+} ions. The analysis based on XRD spectra and the simplified energy diagram suggested that the doped Nd^{3+} ion not only monitored the growth dynamics, but also took an efficient energy transfer of $^4G_{9/2} + {}^7F_0 \rightarrow {}^4I_{9/2} + {}^5D_1$ and a cross relaxation process of $^5D_0 + {}^4I_{15/2} \rightarrow {}^7F_1 + {}^2D_{3/2}$ to generate intense emission from Eu^{3+} ion in both of C_2 and S_6 sites, instead of preferable one type of Eu^{3+} site (C_2 or S_6) in the Nd^{3+} undoped sample.

Acknowledgement A project supported by research fund of Hunan provincial education Department: (2009)192.

References

1. Kang YC, Park SB, Lenggoro IW, Okuyama K (1999) J Mater Res 14(6):2611
2. Kang Y, Roh H, Park S (2000) Adv Mater 12:6
3. Chen X, Yang L, Cook RE, Skanthakumar S, Shi D, Liu GK (2003) Nanotechnology 14:670
4. Bihari B, Eilers H, Tissue BM (1997) J Lumin 75:1
5. Williams DK, Bihari B, Tissue BM, McHale JM (1998) J Phys Chem B 102:916
6. Eilers H, Tissue BM (1996) Chem Phys Lett 251:74
7. Sun L, Qian C, Liao C, Wang X, Yan C (2001) Solid State Commun 119:393
8. Morales Ramírez AJ, Murillo AG, Carrillo Romo FJ, Ramírez Salgado J, Le Luyer C, Chadeyron G, Boyer D (2009) J Moreno Palmerin Thin Solid Films 517:6753

9. Pimputkar S, Speck JS, DenBaars SP, Nakamura S (2009) Nat Photonics 3:180
10. Yang J, Quan Z, Kong D, Liu X, Lin J (2007) Cryst Growth Des 7:730
11. Patra A, Friend CS, Kapoor R, Prasad PN (2002) J Phys Chem B 106:1909
12. Li L, Yang H, Moon B, Choi B, Jeong J, Kim K (2010) Mater Chem Phys 119:471
13. Song HW, Chen BJ (2002) Appl Phys Lett 81:1776
14. Pang Q, Shi J, Liu Y (2003) Mater Sci Eng B 103:57
15. Konrad A, Fries T, Gahn A (1999) J Appl Phys 86:3129
16. Wu CF, Qin WP, Qin GS (2003) Appl Phys Lett 82:520
17. Zhang JL, Hong GY (2004) J Solid State Chem 177:1292
18. Qi ZM, Shi CS (2002) Appl Phys Lett 81:2857
19. Pązik R, Hreniak D, Stręk W, Kessler VG, Seisenbaeva GA (2008) J Alloys Compd 451:557
20. Niraj Luwang M, Ningthoujam RS, Jagannath, Srivastava SK, Vatsa RK (2010) J Am Chem Soc 132:2759
21. Macedo AG, Ananias D, André PS, Sá Ferreira RA, Kholkin AL, Carlos LD, Rocha J (2008) Nanotechnology 19:295702
22. Solarz P (2008) Opt Mater 31:114